CHAPTER 4

VARIATIONAL METHOD FOR ANALYZING SEISMIC STABILITY OF ROCK SLOPES

4.1 INTRODUCTION AND REVIEW OF EXISTING STUDIES

In this chapter, the variational formulations are further extended to provide solutions for the rock slope problems. A number of analytical and numerical studies (Collins et al. 1988; Sonmez et al. 1998; Carranza-Torres 2004; Yang et al. 2004a, 2004b; Yang et al. 2006; Li et al. 2008, 2011; Li et al. 2009; Shen et al. 2013; Lin et al. 2014; Huang et al. 2015; Jiang et al. 2016; Dongping et al. 2017; Belghali et al. 2017; Chen and Lin 2019; Sun et al. 2022) were conducted in the recent past to analyse the homogeneous rock slope subjected to seismic and non-seismic loadings. Collins et al. (1988) investigated the slope stability of closely fractured rocks and rock fill using the upper bound technique and assuming a log-spiral failure mechanism. Sonmez et al. (1998) used back analysis of slope failures to obtain strength parameters of a closely joint rock slope and to explain a practical procedure for evaluating mobilised shear strength and the usefulness of rock mass classification based on the HB failure criterion. Carranza-Torres (2004) proposed a chart for calculating the factor of safety of a 45° sloped rock slope. Under the assumption of a rotational failure mechanism, the upper bound stability factor for rock slope was calculated for the static (Yang et al. 2004a) and pseudostatic (Yang et al. 2004b) cases. Yang et al. (2006) extended the work of rock slope by taking into account the effect of pore water pressure. Li et al. (2008, 2011) employed the finite element limit analysis (FELA) approach to provide rock slope stability charts; Li et al. (2008) thoroughly investigated the accuracy of equivalent Mohr-Coulomb parameters for rock slopes; and Li et al. (2011) investigated

the effect of rock mass disturbance on rock slopes. Chen and Lin (2019) compared the Hoek-Brown (HB) and equivalent Mohr-Coulomb (MC) parameters in slope stability analysis, highlighting their inconsistencies and exploring the sensitivity of HB parameters to factors affecting slope safety factor, such as slope height. Sun et al. (2022) developed a three-dimensional pseudo-dynamic method for seismic stability analysis of rock slopes, considering the temporal and spatial effects of earthquake input. The majority of the numerical and analytical studies were carried out using either the ordinary method of slices or the simplified or modified Bishop method. Most of these studies employed HB failure criterion for modelling the rock mass.

The literature review clearly reveals that the analytical studies correspond to pseudostatic slope stability of rock are quite limited in comparison to static analysis on rock slope and the available studies were based on conventional limit equilibrium method (LEM). However, no literature seems to be found to account the problem of rock slopes by employing variational method. This was the prime motivation to carry out the present work. The objective was to employ variational approach to calculate both the factor of safety and the associated failure surface of a homogeneous rock slope under seismic loading conditions. The Hoek-Brown (HB) criterion was used to model the rock mass. The computed results derived from the analysis were compared to the existing solutions documented in the literature.

4.2 PROBLEM STATEMENT FOR ROCK SLOPE

A rectilinear slope of rock mass, having an angle β, is subjected to seismic forces. The size of the domain, as shown in Fig. 4.1, is kept adequately large so that the slip surface remains within the domain. It is worth mentioning that, in the present analysis, there is no influence on the size of the domain on the computed solutions. The

rock mass is considered homogeneous, isotropic and governed by the HB failure criterion. The rock mass is assumed to be undisturbed (D_f =0) and having unit weight (γ) of 24 kPa for all the cases. The pseudostatic analysis is being carried out for considering the seismic effects; here, the seismic force is assumed to be present only along the horizontal direction (i.e., k_v=0). The objective of this analysis is to determine the critical slip surface corresponding to the critical factor of safety (F_s) for a given rock slope subjected to seismic loadings.

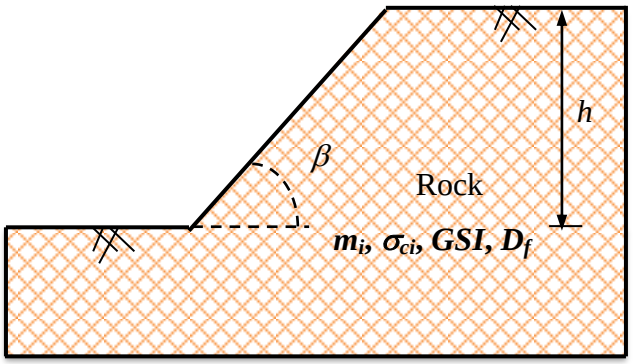

Fig 4.1 Schematic diagram of rectilinear rock slope

4.3 HOEK-BROWN FAILURE CRITERION

By performing a large number of triaxial tests on several rock samples, Hoek and Brown (1980) expressed the following nonlinear relationship between major and minor principal stresses (σ_1 and σ_3) for predicting the rock failure.

$$\sigma_1 = \sigma_3 + \sigma_{ci}\left(m_i \frac{\sigma_3}{\sigma_{ci}} + s\right)^{0.5} \tag{4.1}$$

In this expression, (i) σ_{ci} defines the uniaxial compressive strength of intact rock and (ii) m_i and s are the non-dimensional material strength parameters. The constant m_i, which ranges from 1 to 35, is analogous to the frictional strength of the intact rock and s, which indicates the degree of fracturing of the rock mass, is related to the cohesive

strength of the rock mass. For an intact rock, s=1, and for heavily fractured rock mass; s=0. The original Hoek-Brown failure criterion was later modified for the jointed rock mass and the generalized form of the HB criterion (2002) was proposed as below:

$$\sigma_1 = \sigma_3 + \sigma_{ci}\left(m_b \frac{\sigma_3}{\sigma_{ci}} + s\right)^{\varepsilon} \tag{4.2}$$

Here, the term m_b is introduced to account for the broken rock mass. It indicates the reduced value of the dimensionless material constant m_i. The exponential term ε was introduced so that the curvature of the failure envelope is adjusted to account the strength of poorer quality rock masses in a much better fashion. The constants m_b, ε and s are expressed as the following:

$$m_b = m_i \exp\left(\frac{GSI - 100}{28 - 14D_f}\right) \tag{4.3}$$

$$s = \exp\left(\frac{GSI - 100}{9 - 3D_f}\right) \tag{4.4}$$

$$\varepsilon = \frac{1}{2} + \frac{1}{6}\left(\exp\left(\frac{-GSI}{15}\right) - \exp\left(\frac{-20}{3}\right)\right) \tag{4.5}$$

The parameter *GSI* (Geological Strength Index) can be obtained by the geological observations of the surface quality and interlocking properties. The magnitude of GSI lies between 5 (for highly fractured and poor-quality rock masses) and 100 (for intact rock masses). The disturbance factor (D_f) considers the degree of disturbance of the rock mass. The value of D_f varies from 0 (for undisturbed rock sample) to 1 (for disturbed rock sample). It is to be noted that the isotropic HB criterion is best suited for intact rock and the rock mass having a number of closely spaced discontinuities but without any preferential plane for shearing.

Hoek et al. (2002) proposed an equivalent Mohr-Coulomb (EMC) criterion by fitting an average linear relationship with the generalized HB (GHB) failure envelope. This is done by balancing the areas above and below the EMC plot. This eventually results in the following expressions:

$$\phi_{eq} = \sin^{-1}\left[\frac{6\,\varepsilon\, m_b\left(s + m_b\sigma'_{3n}\right)^{\varepsilon-1}}{2(1+\varepsilon)(2+\varepsilon) + 6\,\varepsilon\, m_b\left(s + m_b\sigma'_{3n}\right)^{\varepsilon-1}}\right] \tag{4.6}$$

$$c_{eq} = \frac{\sigma_{ci}\left[(1+2\varepsilon)s + (1-\varepsilon)m_b\sigma'_{3n}\right]\left(s + m_b\sigma'_{3n}\right)^{\varepsilon-1}}{(1+\varepsilon)(2+\varepsilon)\sqrt{1 + \left(6\varepsilon m_b\left(s + m_b\sigma'_{3n}\right)^{\varepsilon-1}\right)\Big/\left((1+\varepsilon)(2+\varepsilon)\right)}} \tag{4.7}$$

where, (i) ϕ_{eq} and c_{eq} are the equivalent friction angle and cohesive strength, and (ii) $\sigma'_{3n} = \sigma'_{3max}/\sigma_{ci}$

The range of σ_3, within which the matching between the GHB and EMC criteria is done, lies between σ_t ($-s\sigma_{ci}/m_b$) and σ'_{3max}. For slope stability problems, Hoek et al. (2002) proposed the following expression to determine the magnitude of σ'_{3max} which is the upper limit of the confining stress upto which the EMC criterion is matched with the GHB criterion.

$$\frac{\sigma'_{3max}}{\sigma'_{cm}} = 0.72\left[\frac{\sigma'_{cm}}{\gamma h}\right]^{-0.91} \tag{4.8}$$

Here, *h* is the height of the slope and γ is the unit weight of the rock mass. For the stress range of $\sigma_t < \sigma_3 < \sigma_{ci}/4$, the strength of the rock mass, σ'_{cm} can be determined from the following equation.

$$\sigma'_{cm} = \frac{\sigma_{ci}\left(m_b + 4s - \varepsilon(m_b - 8s)\right)\left(m_b/4 + s\right)^{\varepsilon-1}}{2(1+\varepsilon)(2+\varepsilon)} \tag{4.9}$$

Li et al. (2008) proposed a modified expression to determine the value of equivalent cohesive and frictional strength. Depending on the slope angle, Li et al. (2008) obtained the following relationship for improving the estimated factor of safety.

$$\frac{\sigma'_{3max}}{\sigma'_{cm}} = 0.20\left[\frac{\sigma'_{cm}}{\gamma h}\right]^{-1.07} \quad \text{(steep slope, } \beta \geq 45°\text{)} \tag{4.10}$$

$$\frac{\sigma'_{3max}}{\sigma'_{cm}} = 0.41\left[\frac{\sigma'_{cm}}{\gamma h}\right]^{-1.23} \quad \text{(gentle slope, } \beta < 45°\text{)} \tag{4.11}$$

Fig. 4.2 displays the GHB failure envelope (Hoek et al. 2002) and its EMC (Hoek et al. 2002; Li et al. 2008) counterpart for Case A (i.e. m_i=5, and *GSI*=30, 50) and Case B (i.e. m_i=35, and *GSI*=30, 50) corresponding to $\beta < 45°$ and $\beta \geq 45°$. Note the closeness of the EMC envelope proposed by Li et al. (2008) with the GHB envelope.

Although Balmer (1952) has given an analytical solution of normal stress and shear stress by employing the GHB criterion but it becomes a very difficult task to obtain the analytical solutions of the stability problem by applying the GHB criterion defined in terms of normal and shear stresses (Dongping et al. 2017) because whenever Balmer (1952)'s equations will be placed in the equation of factor of safety in LEM expressed as the ratio of shear strength to shear stress an addition term of minor principal stress (σ_3) is appeared to be determined and, hence, the EMC failure criterion has been employed in the present analysis. Eqs. (4.10) and (4.11) are used for selecting the value of σ'_{3max}.

4.4 ANALYSIS

The variational formulations as described in Section 3.3 are duly extended, in the present work, for investigating the stability of any generalized homogeneous rock slope subjected to pseudostatic forces.

By satisfying the static equilibrium conditions (along x and y directions) for each slice, the factor of safety can be expressed as following:

$$F = \frac{\sum_{i=1}^{n} \tau_f}{\sum_{i=1}^{n} \tau_i} = \frac{\sum_{i=1}^{n} \left[c_{eq} + \sigma_{ni} \tan \phi_{eq} \right]}{\sum_{i=1}^{n} \tau_i} = \frac{\sum_{i=1}^{n} \left[c_{eq} \Delta l_i + \left\{ \left(W_i - F_v \right) \cos \theta_i - F_h \sin \theta_i \right\} \tan \phi_{eq} \right]}{\sum_{i=1}^{n} \left(W_i \sin \theta_i + F_h \cos \theta_i - F_v \sin \theta_i \right)} \tag{4.12}$$

The notation of Δx_i, θ_i, Δl_i, W_i, F_v (=$k_v W_i$) and F_h (=$k_h W_i$) are described in section 3.3.1. Similar to the soil slope force distribution of any arbitrary i^{th} slice of rock slope is presented in Fig. 3.2.

By dividing the numerator and the denominator with $\cos\theta_i$ and substituting the expressions of F_v, F_h and Δl_i in Eq. (4.12), the factor of safety can be further expressed as:

$$F = \frac{\sum_{i=1}^{n} \left[c_{eq} \Delta x_i \sec^2 \theta_i + W_i \left\{ \left(1 - k_v \right) - k_h \tan \theta_i \right\} \tan \phi_{eq} \right]}{\sum_{i=1}^{n} W_i \left[\left(1 - k_v \right) \tan \theta_i + k_h \right]} \tag{4.13}$$

The discrete formulation (as shown in Eq. 4.13) is transformed into the continuous form by taking into account the very small width of the slice ($\Delta x_i \to 0$), as illustrated by Revilla and Castillo (1977) and Baker and Garber (1978).

$$F = \lim_{\Delta x_i \to 0} \frac{\sum_{i=1}^{n} \left[c_{eq} \Delta x_i \sec^2 \theta_i + W_i \left\{ \left(1 - k_v \right) - k_h \tan \theta_i \right\} \tan \phi_{eq} \right]}{\sum_{i=1}^{n} W_i \left[\left(1 - k_v \right) \tan \theta_i + k_h \right]} = \frac{\int_{x_0}^{x_n} \left[c_{eq} \left(1 + y_i'^2 \right) + \gamma \left(f_i - y_i \right) \left\{ \left(1 - k_v \right) - k_h y_i' \right\} \tan \phi_{eq} \right] dx}{\int_{x_0}^{x_n} \gamma \left(f_i - y_i \right) \left[\left(1 - k_v \right) y_i' + k_h \right] dx} = \frac{\int_{x_0}^{x_n} P_i(x, y, y') dx}{\int_{x_0}^{x_n} R_i(x, y, y') dx} \tag{4.14}$$

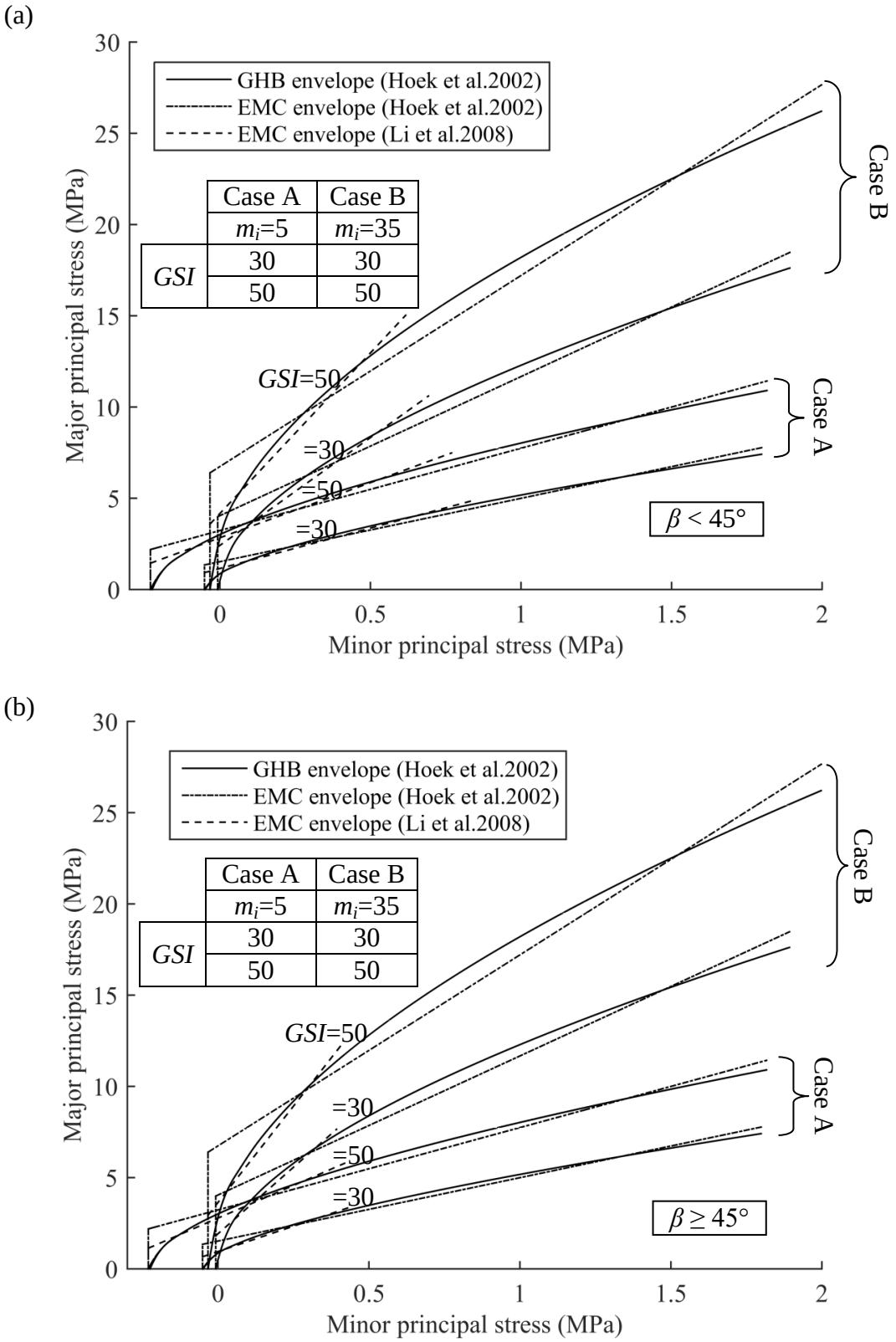

Fig. 4.2 Graphical representation of GHB (Hoek et al. 2002) and EMC (Hoek et al. 2002; Li et al. 2008) for different *GSI* and m_i corresponding to (a) $\beta < 45°$ and (b) $\beta \geq 45°$.

Similar to the homogeneous soil slope (Case 1) (as depicted in chapter 3) the rock slope can also be divided into three regions (as shown in Fig. 3.3a). The mathematical expressions for the homogeneous rock slope surface within these regions are identical to the homogeneous soil slope that is demonstrated in Table 3.2 for Case 1. These equations are not repeated herein.

Corresponding to each $f_i(x)$ there would be a distinct $y_i(x)$ in the interval of (x_{i-1}, x_i) (as illustrated in Fig. 3.3a). The expression of factor of safety in Eq. (4.14) takes the similar form as depicted in Eq. (3.8). The functionals (F) that is mentioned in Eq. (3.8) are required to minimized to obtain critical slip surface and corresponding critical factor of safety (F_s). The minimization process is being performed by using Euler-Lagrangian equation as depicted in Eq. (3.10).

By applying Euler-Lagrangian equation the expression of critical factor of safety for homogeneous rock slope can be presented as follows:

$$F_s = \frac{2c_{eq}y_i'' + \gamma \tan\phi_{eq}\left[\left(1-k_v\right) - f_i'\,k_h\right]}{\gamma\left[\left(1-k_v\right)f_i' + k_h\right]};\ \left(i = 1,2,3\right) \tag{4.15}$$

From Eq. (4.15), the slip surface for three different ranges, can be obtained. All three surfaces are presented in Fig. 3.3a. The three surfaces are as follows:

$$\text{Where}\ \begin{cases} y_i = A_i x^2 + B_i x + D_i\,; \quad (i=1,\,2,\,3) \\ A_1 = A_3 = -\dfrac{\gamma}{4c_{eq}}\tan\phi_{eq}\left(1-k_v\right) + \dfrac{\sigma_{ci}k_h}{4c_{eq}Nh} \\ A_2 = -\dfrac{\gamma}{4c_{eq}}\tan\phi_{eq}\left\{\left(1-k_v\right) - \dfrac{h}{h_1}k_h\right\} + \dfrac{\sigma_{ci}}{4c_{eq}Nh}\left\{\left(1-k_v\right)\dfrac{h}{h_1} + k_h\right\} \end{cases} \tag{4.16}$$

Here, $N\left(=\sigma_{ci}/F_s\gamma h\right)$ indicates the dimensionless stability number.

Similar to the homogeneous soil slope, the slip surface equation for homogeneous rock slope consists of two integration constants (B_i's and D_i's). As a

result, the total number of unknown parameters becomes nine- (i) two endpoints (x_0 and x_3), (ii) F_s and (iii) six integration constants (B_1, B_2, B_3, D_1, D_2 and D_3).

Fortunately, the transversality, continuity, natural boundary and intersection condition provide with nine known equations. Hence, the problem becomes well defined, as demonstrated in Section 3.3.6. The nine unknown parameters are evaluated with the aid of these equations. The expressions for the unknown parameters are as follows:

$$B_1 = B_2 = -1 + \frac{\gamma x_0}{2c_{eq}} \tan\phi_{eq}(1-k_v) - \frac{\sigma_{ci} k_h}{2c_{eq} N h} x_0 \tag{4.17}$$

$$B_3 = 1 + \frac{\gamma x_3}{2c_{eq}} \tan\phi_{eq}(1-k_v) - \frac{\sigma_{ci} k_h}{2c_{eq} N h} x_3 \tag{4.18}$$

$$D_1 = D_2 = x_0 - \frac{\gamma x_0^2}{4c_{eq}} \tan\phi_{eq}(1-k_v) + \frac{\sigma_{ci} k_h x_0^2}{4c_{eq} N h} \tag{4.19}$$

$$\begin{aligned} D_3 = {} & \frac{\gamma h h_1}{4c'} \tan\phi_{eq} k_h + \frac{\sigma_{ci} h_1 (1-k_v)}{4c_{eq} N} - 2h_1 + x_0 - \frac{\gamma h_1 \tan\phi_{eq}(1-k_v)(x_3 - x_0)}{2c_{eq}} \\ & + \frac{\sigma_{ci} h_1 k_h (x_3 - x_0)}{2c_{eq} N h} - \frac{\gamma x_0^2 \tan\phi_{eq}(1-k_v)}{4c_{eq}} + \frac{\sigma_{ci} k_h x_0^2}{4c_{eq} N h} \end{aligned} \tag{4.20}$$

$$N = \frac{\sigma_{ci}\left[(1-k_v) + \frac{k_h}{h}(x_3 - x_0)\right]}{\left[4c_{eq} - \gamma h k_h \tan\phi_{eq} + \gamma \tan\phi_{eq}(1-k_v)(x_3 - x_0)\right]} \tag{4.21}$$

$$x_3 = \frac{-B \pm \sqrt{B^2 - 4AC}}{2A} \tag{4.22}$$

It is worth mentioning that the form of the slip surface is the combination of the three planes, namely, y_1, y_2 and y_3, which are obtained through the analytical solution of Eq. (4.16) by satisfying the required constraints. Following the work of Yang et al. (2004b), Li et al. (2008) and Dong-Ping et al. (2017), in the present case, the

homogeneous rock slope ($\beta \geq 35^0$) subjected to pseudostatic force is assumed to fail by developing toe failure surface (x_0=0).

For x_0= 0 the expressions of *A*, *B* and *C* in Eq. (4.22) takes the following form.

$$A = \frac{\gamma h}{4c_{eq}} \tan\phi_{eq}\left(1-k_v\right)^2 + \frac{\gamma h}{4c_{eq}} \tan\phi_{eq} k_h^2 \tag{4.23}$$

$$B = h\left(1-k_v\right) - hk_h - \frac{\gamma h h_1 \tan\phi_{eq} k_h^2}{4c_{eq}} - \frac{\gamma h h_1 \tan\phi_{eq}\left(1-k_v\right)^2}{4c_{eq}} \tag{4.24}$$

$$C = -hh_1\left(1-k_v\right) - h^2\left(1-k_v\right) \tag{4.25}$$

Note that the non-dimensional stability number (*N*), an inverse indicator of F_s, becomes a function of all the considered input parameters. In the results and discussion section for rock slope, the entire discussions are being done in terms of F_s.

4.5 RESULTS AND DISCUSSIONS

In the present study, some typical homogeneous rock slopes are analyzed for different geometrical, material and loading parameters as mentioned below:

Geometrical Properties: (i) Slope height (*h*=20 and 100 m);

(ii) Slope inclination angle (β=35° to 75° with a 20° interval)

Material Properties: (i) Uniaxial compressive strength of the intact rock (σ_{ci} =25, 50, and 250 MPa)

(ii) Geological strength index (*GSI*=10, 30, 50, and 100)

(iii) m_i (= 5, 20, and 35)

Loading Conditions: (i) Horizontal seismic coefficient (k_h= 0.0, 0.2, and 0.4)

The numerical values of those input parameters have been considered with wide possible ranges after thorough study of available previous literatures (Li et al. 2008, 2011; Shen et al. 2013; Jiang et al. 2016). The obtained solutions for different combination of rock properties (σ_{ci}, *GSI* and m_i) and slope geometries subjected to different horizontal seismic forces are reported in Tables 4.1 and 4.2; Table 4.1 presents the solutions for h=20 m and Table 4.2 presents the solutions for h=100 m. Variation in slope geometry, rock properties and loading conditions also have a pronounced impact on the size and shape of the critical slip surface and, hence, the critical slip surfaces are drawn and discussed in the following section for few cases.

4.5.1 Influence of slope geometry (β and h)

It is well observed from Tables 4.1 and 4.2 that the magnitude of F_s reduces with an increase in slope height (h) as well as slope inclination angle (β). Fig. 4.3 shows the variation of F_s with m_i for different values of *GSI* corresponding to β =35° and β =75°. The figure suggests that if the rock medium is not subjected to any seismic loadings, the impact of β is significantly higher for lower values of *GSI*, however, for higher *GSI* (say for, *GSI* =100) there is hardly any difference of computed F_s between the steep slopes and gentle slopes. As the horizontal seismic force increases (say for, k_h= 0.4), the deviation of F_s for different slope angle is clearly observable even for higher *GSI*. The obtained solutions suggest that the % reduction in F_s values due to the increase in slope height is not further significantly affected by β and k_h.

The effect of slope height in reducing the safety factor does not seem to be dependent much on slope angle and horizontal seismic coefficient. For an example, for a certain rock slope (β =35°, m_i = 5, *GSI*=10 and σ_{ci} =25) when the value of h increases from 20 m to 100 m, F_s reduces by (i) 35.2% in static case (k_h=0), and (ii) 37.6% in

pseudostatic case (k_h=0.4). For the same rock medium, if the slope is steep (for β=75°), the same increment of h (from 20 m to 100 m) suppresses F_s by (i) 39.06% in static case (k_h=0), and (ii) 42.08% in pseudostatic case (k_h=0.4). Figs. 4.4 and 4.5 show the form of the critical slip surface for different slope angles (β=55° and 75°) and different slope height (h=20 m and 100 m). The shape of the slip surfaces appears to be highly dependent on the geometric profile of the slope. As the slope becomes steep, there is an appreciable reduction in the volume of the rock mass contains within the slip surface. With the increase in the height of the slope, the horizontal extent and overall size of the critical slip surface increases to a considerable amount.

4.5.2 Influence of rock properties (m_i, *GSI* and σ_{ci})

Tables 4.1 and 4.2 depict clearly that for a constant m_i, F_s improves drastically with the rise in *GSI* value. However, for a constant value of *GSI*, the variation of F_s with the increase in m_i does not follow a persistent trend; for lower values of *GSI* (=10, 30 and 50) the curve between F_s and m_i shows an increasing trend while for *GSI*=100, the pattern is decreasing in nature. This reversal of trend can be attributed to the fact that the pattern of c_{eq}/σ_{ci} - m_i – *GSI* graph changes beyond a specific value of *GSI*, which is termed here as GSI_{sp}. A similar observation was also reported by Hoek and Brown (1997). Fig. 4.6 shows the graph between c_{eq}/σ_{ci} and *GSI* for different values of m_i. Table 4.3 shows that the value of GSI_{sp} depends upon slope geometry and σ_{ci}.

This table suggests that GSI_{sp} is highly influenced by the slope height but not much dependent on the slope angle. This indicates that for a very good quality rock mass (i.e., *GSI*=100) and a certain σ_{ci}, equivalent cohesion decreases with increase in m_i and this eventually results in the reduction of F_s. Jiang et al. (2016) also reported that

Table 4.1 The values of F_s for h= 20m and corresponding to different β, σ_{ci}, GSI, m_i and k_h

			β=35°			β=55°			β=75°		
σ_{ci} (MPa)	k_h	m_i / GSI	5	20	35	5	20	35	5	20	35
25	0.00	10	1.4	2.2	2.7	0.9	1.4	1.7	0.6	0.9	1.1
		30	2.6	3.5	4.0	1.9	2.3	2.6	1.4	1.7	1.8
		50	4.4	5.0	5.4	3.7	3.6	3.8	3.2	2.8	2.9
		100	51.8	31.3	26.2	51.1	30.0	24.5	50.8	29.2	23.5
	0.20	10	1.0	1.5	1.8	0.7	1.0	1.2	0.5	0.6	0.7
		30	1.8	2.4	2.8	1.4	1.7	1.9	1.1	1.2	1.3
		50	3.1	3.5	3.8	2.8	2.7	2.8	2.6	2.1	2.1
		100	38.9	22.8	18.5	36.3	21.9	18.2	32.8	20.6	17.6
	0.40	10	0.7	1.1	1.3	0.5	0.7	0.8	0.3	0.4	0.4
		30	1.3	1.7	2.0	1.0	1.2	1.3	0.8	0.8	0.8
		50	2.3	2.5	2.7	2.2	2.0	2.0	2.0	1.6	1.5
		100	28.4	17.4	14.4	25.1	15.9	13.5	21.1	14.1	12.4
50	0.00	10	1.7	2.6	3.1	1.2	1.7	2.0	0.8	1.1	1.3
		30	3.4	4.3	4.9	2.6	2.9	3.2	2.1	2.2	2.3
		50	6.8	6.7	7.0	5.9	5.1	5.1	5.4	4.2	4.0
		100	101.5	58.4	47.2	100.9	57.1	45.4	100.5	56.2	44.3
	0.20	10	1.2	1.8	2.2	0.8	1.2	1.4	0.6	0.8	0.9
		30	2.4	3.0	3.4	2.0	2.1	2.3	1.7	1.6	1.6
		50	4.7	4.7	4.9	4.5	3.8	3.8	4.3	3.3	3.1
		100	76.6	43.4	34.5	71.2	40.9	33.0	63.8	37.6	30.9
	0.40	10	0.9	1.3	1.5	0.6	0.8	0.9	0.4	0.4	0.5
		30	1.8	2.2	2.4	1.5	1.5	1.6	1.3	1.1	1.1
		50	3.5	3.4	3.6	3.5	2.9	2.8	3.4	2.5	2.3
		100	55.4	32.3	26.1	48.4	28.9	23.8	40.1	24.8	21.0
250	0.00	10	3.2	4.1	4.7	2.4	2.7	3.0	1.9	2.0	2.1
		30	8.3	8.1	8.5	7.3	6.2	6.1	6.7	5.1	4.9
		50	23.2	16.5	15.4	22.1	14.5	12.9	21.5	13.4	11.5
		100	499.1	274.1	212.5	498.4	272.7	210.7	498.0	271.9	209.6
	0.20	10	2.2	2.8	3.3	1.8	2.0	2.1	1.5	1.4	1.4
		30	5.8	5.7	5.9	5.5	4.6	4.6	5.3	4.0	3.7
		50	16.8	11.4	10.8	16.2	11.0	9.8	15.3	10.7	9.2
		100	378.5	207.2	160.1	350.2	192.4	149.2	311.2	172.0	134.1
	0.40	10	1.6	2.0	2.3	1.4	1.4	1.5	1.1	0.9	0.9
		30	4.3	4.2	4.3	4.3	3.5	3.4	4.2	3.1	2.7
		50	12.8	8.5	7.9	11.8	8.4	7.6	10.5	8.3	7.4
		100	270.9	149.4	116.3	234.8	130.4	102.0	192.0	107.7	85.1

Table 4.2 The values of F_s for h= 100m and corresponding to different β, σ_{ci}, GSI, m_i and k_h

			β=35°			β=55°			β=75°		
σ_{ci} (MPa)	k_h	m_i / GSI	5	20	35	5	20	35	5	20	35
25	0.00	10	0.9	1.5	1.8	0.6	0.9	1.1	0.4	0.6	0.9
		30	1.4	2.2	2.6	1.0	1.5	1.7	0.7	1.0	1.4
		50	2.1	2.9	3.3	1.5	1.9	2.2	1.2	1.4	2.1
		100	11.9	9.0	8.6	11.3	7.9	7.2	10.9	7.2	11.9
	0.20	10	0.6	1.0	1.3	0.4	0.7	0.8	0.3	0.4	0.6
		30	1.0	1.5	1.8	0.7	1.0	1.2	0.5	0.7	1.0
		50	1.5	2.0	2.3	1.1	1.4	1.6	0.9	1.0	1.5
		100	8.6	6.2	6.0	8.3	6.0	5.5	7.9	5.8	8.6
	0.40	10	0.4	0.7	0.9	0.3	0.5	0.6	0.2	0.3	0.4
		30	0.7	1.1	1.3	0.5	0.7	0.8	0.3	0.5	0.7
		50	0.9	1.5	1.8	0.6	0.9	1.1	0.4	0.6	0.9
		100	1.4	2.2	2.6	1.0	1.5	1.7	0.7	1.0	1.4
50	0.00	10	1.1	1.8	2.1	0.7	1.1	1.3	0.5	0.8	1.1
		30	1.8	2.7	3.1	1.3	1.8	2.0	0.9	1.2	1.8
		50	2.8	3.6	4.1	2.1	2.5	2.7	1.8	1.8	2.8
		100	21.9	14.8	13.3	21.3	13.6	11.7	20.9	12.8	21.9
	0.20	10	0.7	1.2	1.5	0.5	0.8	0.9	0.3	0.5	0.7
		30	1.3	1.9	2.2	0.9	1.3	1.5	0.7	0.9	1.3
		50	2.0	2.5	2.8	1.6	1.8	2.0	1.4	1.3	2.0
		100	16.2	10.2	9.2	15.3	10.1	8.9	14.2	10.0	16.2
	0.40	10	0.5	0.9	1.1	0.3	0.5	0.6	0.2	0.3	0.5
		30	0.9	1.3	1.6	0.7	0.9	1.0	0.5	0.6	0.9
		50	1.4	1.8	2.0	1.2	1.3	1.4	1.0	0.9	1.4
		100	12.1	8.0	6.9	10.9	7.7	6.8	9.5	7.2	12.1
250	0.00	10	1.7	2.6	3.1	1.2	1.7	2.0	0.8	1.1	1.3
		30	3.4	4.3	4.9	2.6	2.9	3.2	2.1	2.2	2.3
		50	6.8	6.7	7.0	5.9	5.1	5.1	5.4	4.2	4.0
		100	101.5	58.4	47.2	100.9	57.1	45.4	100.5	56.2	44.3
	0.20	10	1.2	1.8	2.2	0.8	1.2	1.4	0.6	0.8	0.9
		30	2.4	3.0	3.4	2.0	2.1	2.3	1.7	1.6	1.6
		50	4.7	4.7	4.9	4.5	3.8	3.8	4.3	3.3	3.1
		100	76.6	43.4	34.5	71.2	40.9	33.0	63.8	37.6	30.9
	0.40	10	0.9	1.3	1.5	0.6	0.8	0.9	0.4	0.4	0.5
		30	1.8	2.2	2.4	1.5	1.5	1.6	1.3	1.1	1.1
		50	3.5	3.4	3.6	3.5	2.9	2.8	3.4	2.5	2.3
		100	55.4	32.3	26.1	48.4	28.9	23.8	40.1	24.8	21.0

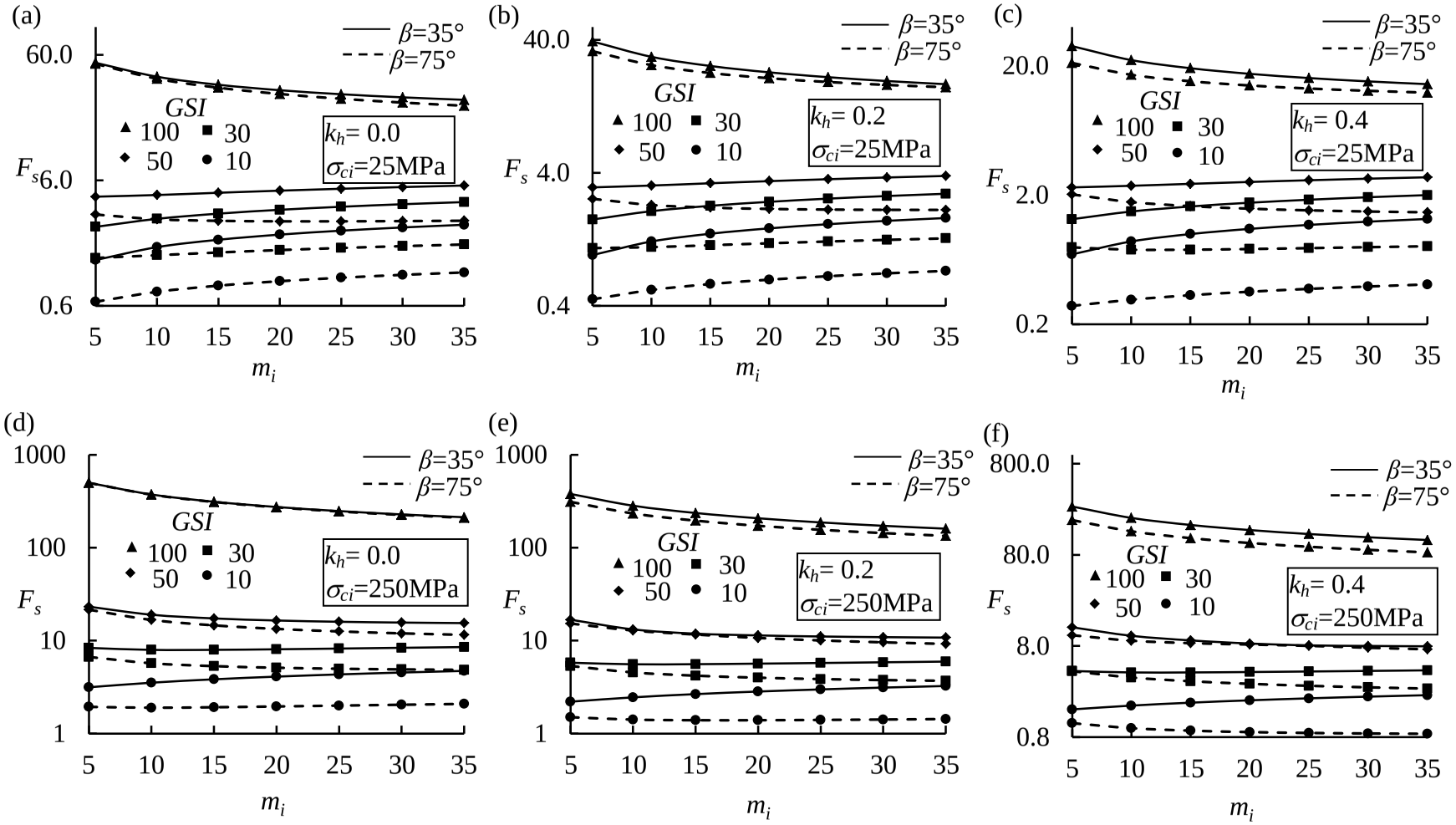

Fig 4.3 The variation of F_s with mi for h=20m with k_h equals to (a, d) 0.0; (b, e) 0.2 and (c, f) 0.4 correspond to two σ_{ci}, namely, 25 and 250 Mpa.

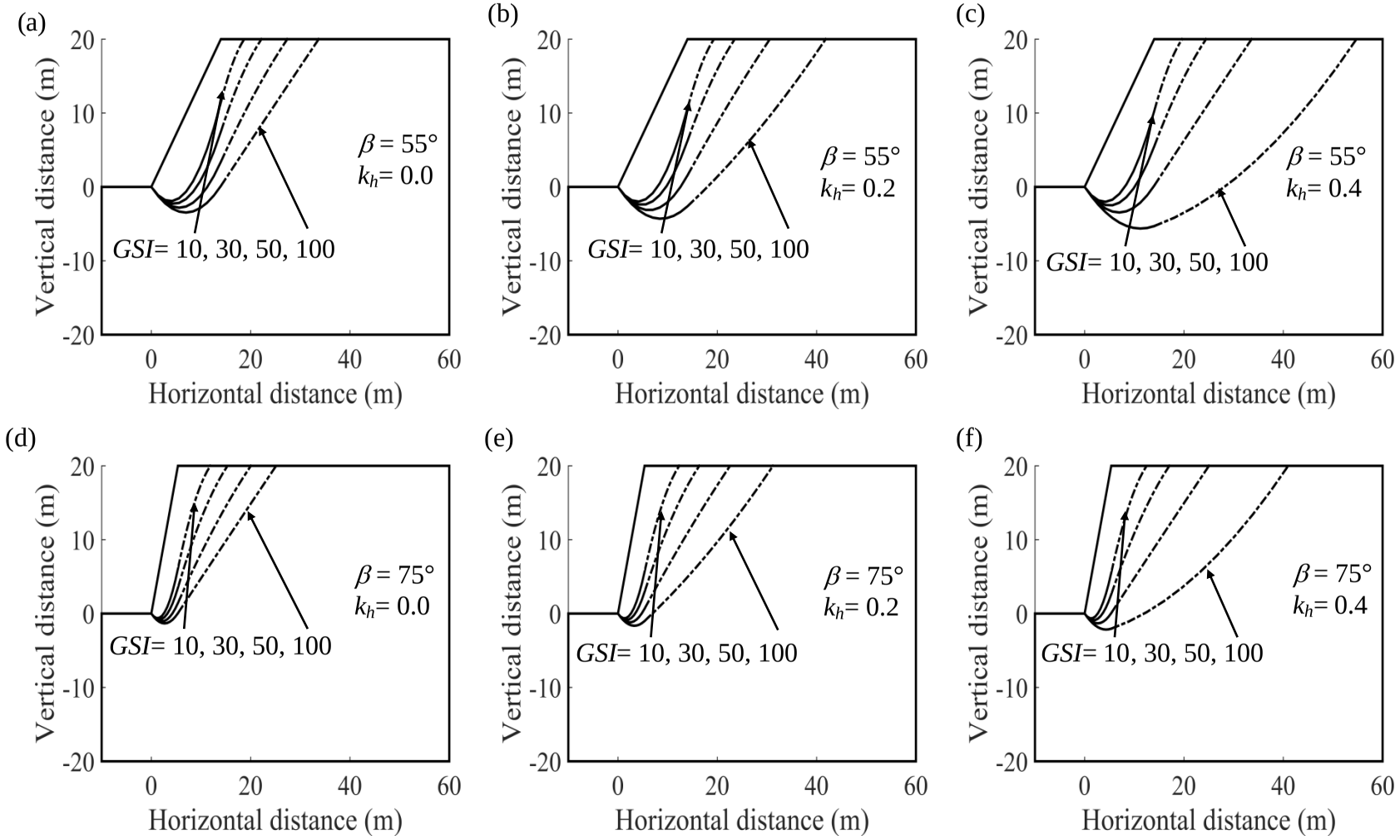

Fig 4.4 Form of the critical slip surfaces for h=20m with k_h equals to (a, d) 0.0; (b, e) 0.2 and (c, f) 0.4 and correspond to two β, namely, 55° and 75°.

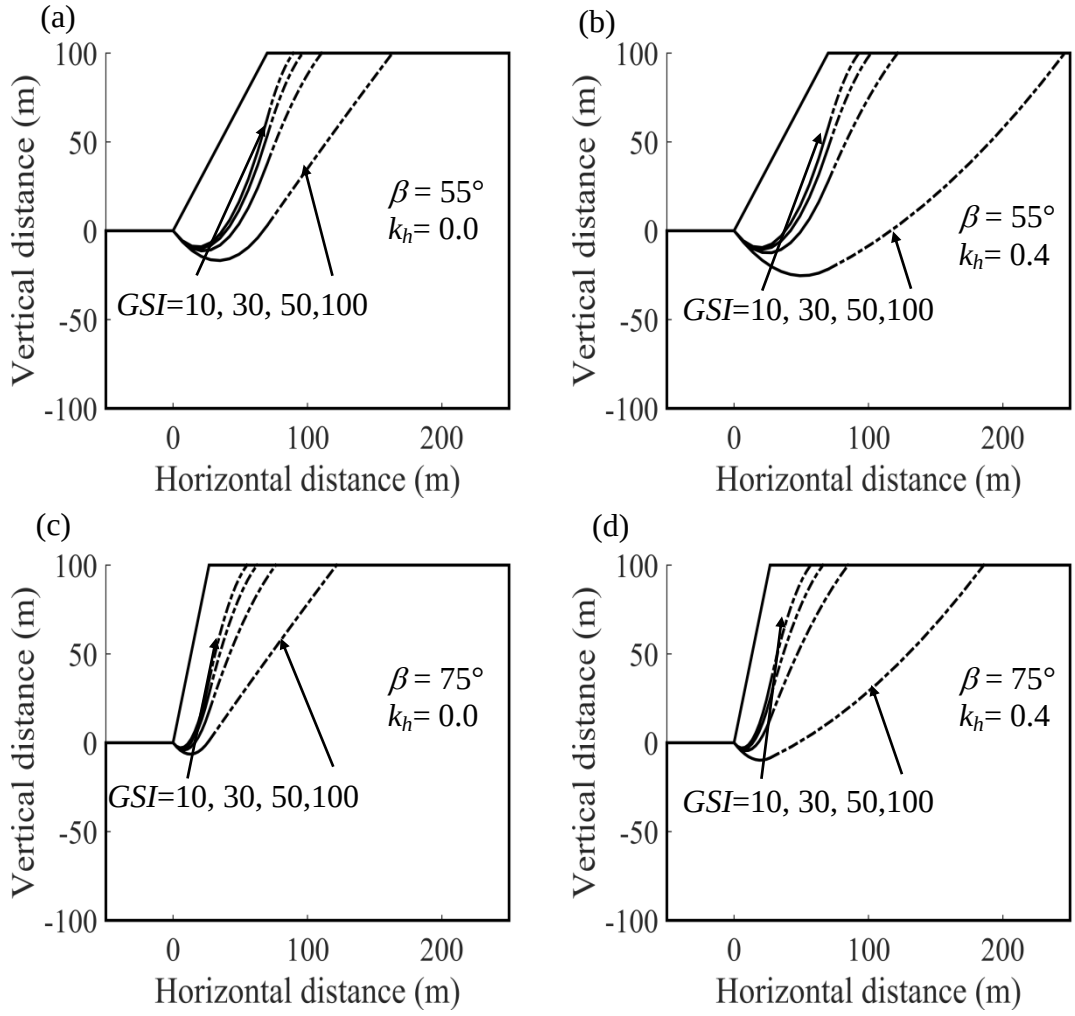

Fig 4.5 Form of the critical slip surfaces for h=100m with (a) β=55°, k_h=0; (b) β=55°, k_h=0.4; (c) β=75°, k_h=0; and (d) β=75°, k_h =0.4.

the rock slope having high *GSI* values and subjected to seismic forces collapses due to tension failure and due to which F_s reduces with increase in m_i.

The magnitude of σ_{ci} also impacts immensely on the computed safety factors of the rock slope. Higher the σ_{ci}, better is the stability of the slope. Fig 4.3 displays the variation of F_s with m_i for two different values of σ_{ci}, namely, 25 and 250 MPa. It suggests that when the value of σ_{ci} equals to 250 MPa the reversal of the trend of the curve between F_s and m_i starts to happen even for lower values of *GSI*. Table 4.4 shows the percentage increase in F_s by increasing the σ_{ci} in two different ways – (i) from 25 to 50 MPa and (ii) from 25 to 250 MPa. It can be inferred from the table that for certain

slope geometry, the percentage increment in F_s (a) increases further with *GSI* (for a specific m_i) but (b) decreases with increase in m_i (while *GSI* is kept to be constant). These values also reveal that increment in σ_{ci} is much beneficial for steep slopes and smaller slope height. Fig. 4.7 depicts that the increment of σ_{ci} enlarges the size of the critical slip surface especially for the rocks having lower *GSI*.

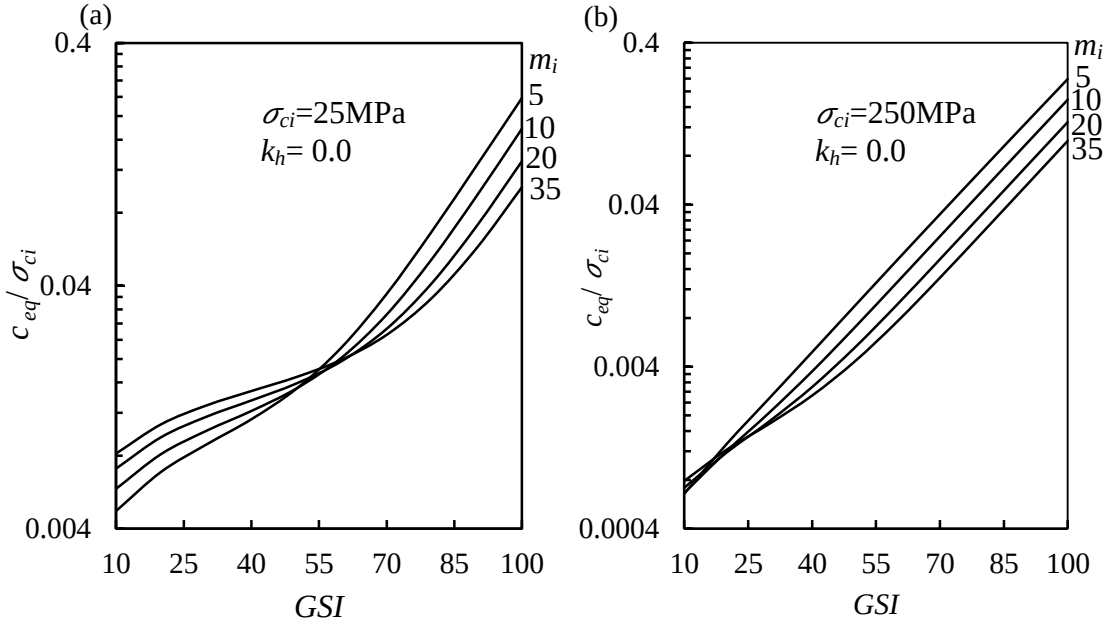

Fig 4.6 The variation of c_{eq}/σ_{ci} with *GSI* and m_i for σ_{ci} equals to (a) 25 MPa and (b) 250 MPa.

Table 4.3 The values of GSI_{sp} for different β, h and σ_{ci}

	β=35°		β=75°	
σ_{ci} (MPa)	h=20m	h=100m	h=20m	h=100m
25	30	58	28	51
50	20	44	18	40
250	–	18	–	17

Figs. 4.4, 4.5 and 4.7 illustrate that the critical slip surface grows in size with the increment of *GSI* value. This observation is in the same line as reported in the work of Li et al. (2008, 2011). The difference in the size of the critical slip surface between *GSI*=10 and *GSI*=100 becomes more prominent for higher k_h (say for, k_h=0.4). The magnitude of *GSI* also impacts the curvature of the failure surfaces. Figs. 4.4 and 4.5 also show that with the increase of slope angle, the size and curvature of the slip surface decreases. Fig. 4.7 depicts that for certain slope geometry and *GSI*, higher the magnitude of σ_{ci} higher is the horizontal extent of the critical slip surface. It has been observed that the variation of m_i does not affect much on the size and shape of the critical slip surface and, hence, these surfaces are not being reported in the present work.

4.5.3 Influence of horizontal seismic forces (k_h)

Incorporating the seismic acceleration in the analysis reduces the factor of safety to a considerable extent. Table 4.5 shows the percentage reduction in the computed F_s when k_h varies from (i) 0.0 to 0.2 and (ii) 0.0 to 0.4. The reported data give an impression that for gentle slope the percentage reduction in F_s not at all depends upon the slope height, *GSI*, m_i and σ_{ci}. However, for the steep slope, there is an impact of the slope height and rock properties on the amount of reduction in F_s. Figs. 4.4 and 4.5 show that for certain rock mass, horizontal seismic force enhances the size of the slip surfaces, irrespective of slope geometries, resulting in a higher amount of soil within the slip surface.

Table 4.4 The percentage increase in F_s of the rock slope on account of the increase in σ_{ci}

	% increase in F_s when σ_{ci} increases from 25 to 50MPa				% increase in F_s when σ_{ci} increases from 25 to 250MPa			
	β =35°		β =75°		β =35°		β =75°	
GSI	h =20 m	h =100 m	h =20 m	h =100 m	h =20 m	h =100 m	h =20 m	h =100 m
10	23.7 (18.1)	23.5 (18.3)	31.3 (18.2)	23.1 (16.9)	126.6 (78.1)	102.3 (73.9)	203.1 (89.1)	115.4 (68.8)
50	52.5 (29.4)	34.3 (22.7)	68.1 (41.8)	48.3 (26.1)	421.9 (183.6)	227.0 (112.7)	572.2 (304.6)	356.0 (157.3)
100	96.0 (79.8)	84.7 (55.0)	98.0 (756.5)	91.4 (70.5)	863.8 (710.0)	881.0 (451.7)	88.4 (790.2)	819.2 (599.4)

Note: The values within and outside the parenthesis are for the rock mass having m_i equals to 35 and 5, respectively.

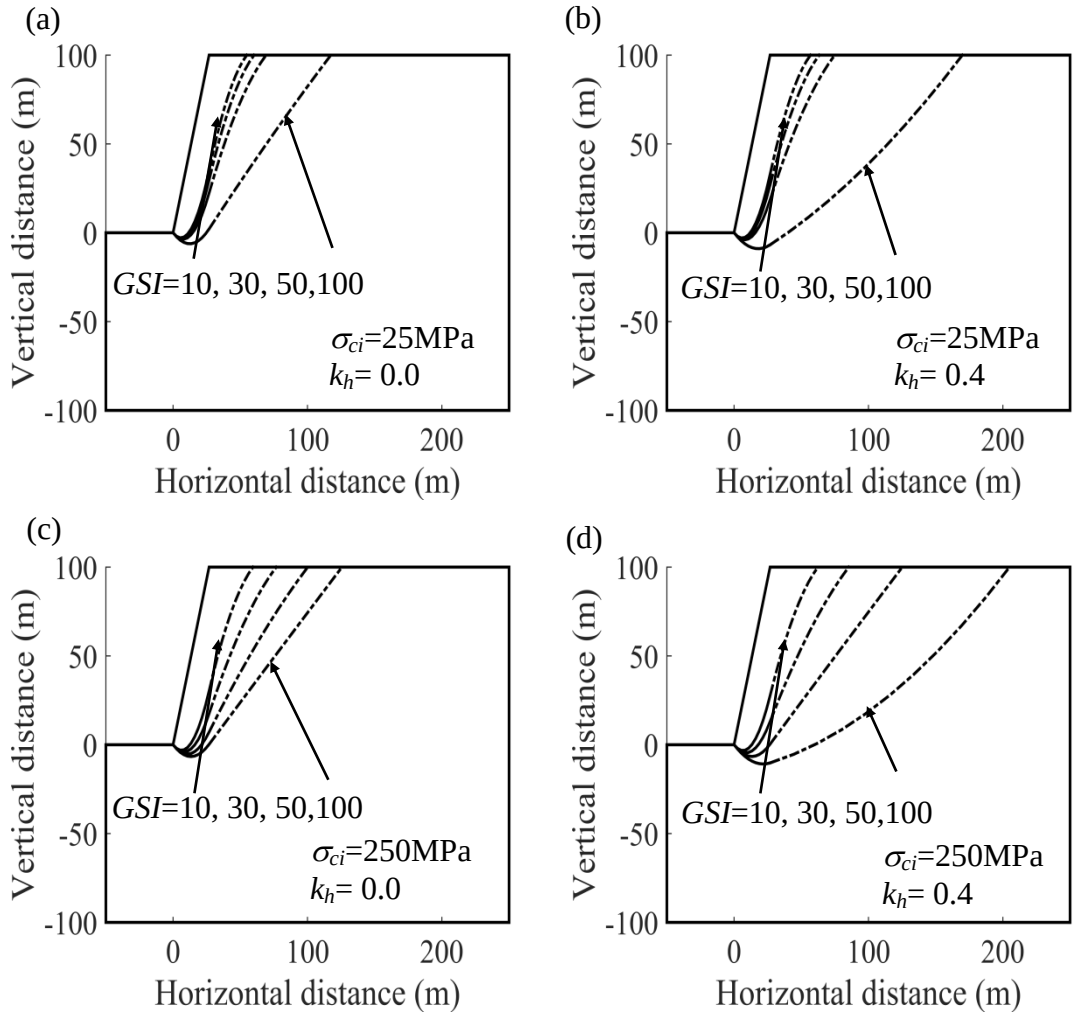

Fig. 4.7 Form of the critical slip surfaces for h=100m and β=75° with (a) σ_{ci}=25MPa, k_h=0; (b) σ_{ci}=25MPa, k_h=0.4; (c) σ_{ci}=250MPa, k_h=0; and (d) σ_{ci}=250MPa, k_h =0.4.

4.6 COMPARISON OF RESULTS

4.6.1 Comparison of the solutions obtained by Hoek et al. (2002)'s and Li et al. (2008)'s proposition regarding σ'_{3max}

Fig 4.8 shows the comparisons of the predicted safety factor by adopting different definition of σ'_{3max}. As expected, applying Eq. (4.8) instead of Eqs. (4.10-4.11) suppresses the estimation of F_s to a considerable extent. This suppression is further influenced by the slope inclination angle and the rock properties. As the slope becomes steeper and m_i increases, the percentage difference between these two solutions becomes quite significant. The reduction of the computed F_s value also gets affected by

Table 4.5 The percentage decrease in F_s of the rock slope on account of the increase in k_h

		% decrease in F_s when k_h varies from 0 to 0.2				% decrease in F_s when k_h varies from 0 to 0.4			
		β=35°		β=75°		β =35°		β=75°	
m_i	Case	h =20 m	h =100 m	h =20 m	h =100 m	h =20 m	h =100 m	h =20 m	h =100 m
5	I	30.9 (30.2)	30.6 (29.9)	29.7 (20.3)	30.8 (24.6)	50.4 (48.4)	49.4 (48.8)	56.3 (36.9)	59.0 (44.9)
35	II	30.3 (30.1)	30.5 (30.5)	26.3 (24.0)	29.3 (28.8)	49.6 (49.0)	49.6 (49.8)	48.4 (43.8)	54.1 (53.0)

Note: (a) Case-I: The rock mass having the same σ_{ci} (=25 MPa) but different *GSI*; the values within and outside the parenthesis are for rock having *GSI* = 50 and 10, respectively.

(b) Case-II: The rock mass having the same *GSI* (=50) but different σ_{ci}; the values within and outside the parenthesis are for σ_{ci} = 50 and 25, respectively.

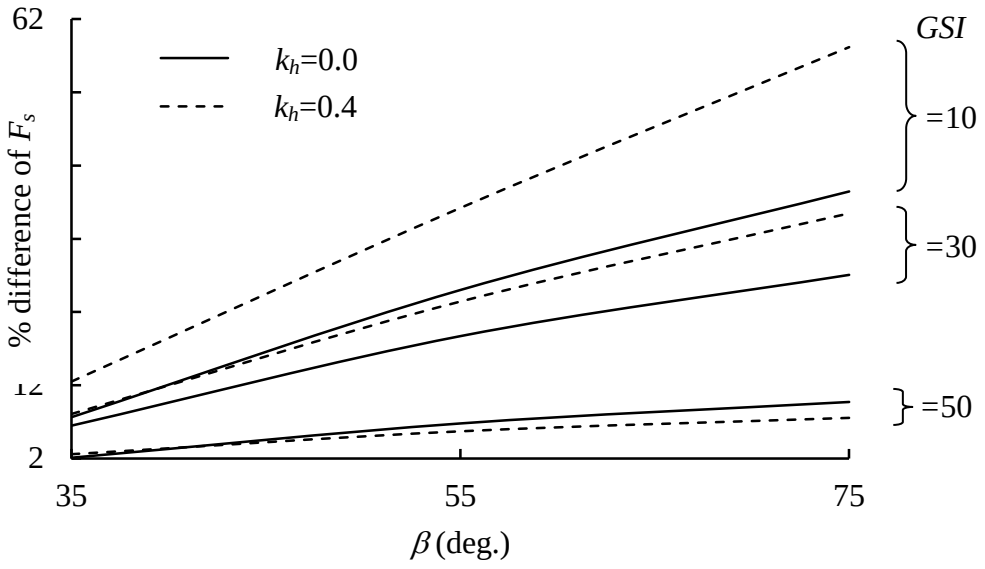

Fig. 4.8 Percentage difference of F_s by using formulation of Hoek et al. (2002) and Li et al. (2008) with β for different *GSI* corresponding to varying k_h with σ_{ci}=250 MPa.

the increase in k_h and σ_{ci} values. For a slope of 75° angle with *GSI*=10, m_i =35 and σ_{ci}=250 MPa, Li et al.'s (2008) formulation reduces the estimation of F_s (from Hoek et al. 2002) by 62.50%. This reduction of F_s is highly encouraging in the sense that the parameter of the EMC criterion obtained by Eq. (4.8) can overestimate the magnitude of F_s even by 64%, as reported by Li et al. (2008). Hence, this comparison clearly shows that using Li et al.'s (2008) expression of computing σ'_{3max} is far more beneficial for estimating the parameters of EMC criterion especially for steep slopes and poor-quality rock masses. However, for good quality rock (i.e., *GSI*=100 and high σ_{ci}), both the equations provide the same value of the equivalent parameters.

4.6.2 Comparison of the present solutions with the solutions available in the literature

In order to understand the accuracy of the proposed design charts, the factor of safety obtained from the present analysis are compared with the solutions available in

the literature. Table 4.6 presents the comparisons of the present values with the solutions reported by Carranza-Torres (2004), Li et al. (2011) and Shen et al. (2013) for different rock slopes with different geometry, material and loading properties. Carranza-Torres (2004) and Shen et al. (2013) used LEM and Li et al. (2011) used FELA for analyzing different slopes. The trend of the present solutions agrees well with the LEM solutions. The magnitude of F_s as reported by Carranza-Torres (2004) are on the higher side due to the consideration of ε=0.5. The deviation between the solutions obtained by FELA and the present method can be attributed to the fact that Li et al. (2011) computed the factor of safety from the stability number and not from the definition of the ratio of the resisting force to the disturbing force.

The present results are further compared with the solutions provided by Li et al. (2008) and Dong-Ping et al. (2017) for three different β, namely, 30°, 45° and 60° correspond to varying m_i values and constant *GSI* (=100). Li et al. (2008) analyzed the slope by using FELA method and had obtained the optimum unit weight considering the state when the collapse state has just occurred (i.e. F_s=1). This eventually provided the critical non-dimensional strength ratio $(\sigma_{ci}/(\gamma h))_{cr}$, which is considered as a reference for the comparisons, as presented in Table 4.7. The present method seems to estimate conservative solutions. Similar kind of underestimation of the stability numbers are also reported for the soil slopes analyzed with the variational method (Baker and Garber 1978; Castillo and Luceno 1982; Leshchinsky and San 1994; Baker et al. 2006). This further provides the confidence in the present computed solutions.

Table 4.8 shows the comparisons of the computed F_s from the present analysis with the solution of (i) Lin et al. (2014) based on modified Bishop method and (ii) Huang et al. (2015) on the basis of ordinary method of slice. The comparisons were carried out for two different cases – (a) altering the magnitude of m_i while *GSI* is kept

to be constant and (b) varying *GSI* for a given m_i. The trends match quite well; however, the present solutions are smaller than the solutions reported by Lin et al. (2014) and Huang et al. (2015). Tables 4.6, 4.7 and 4.8 present the comparison solely for the static cases (k_h = 0). Table 4.9 depicts the comparison of the enumerated F_s obtained from present analysis with the available solution of Chen and Lin (2019) correspond to varying (i) slope height (h) and (ii) material properties of the rock masses (σ_{ci}, *GSI* and m_i) for β=60°. The trend of both the results match quite well; however, the present numerical values are quite smaller than that of Chen and Lin's (2019) solution. The reason can be attributed to the fact that the gravity increase method employed by Chen and Lin (2019) overestimates the stability value significantly (Sternik 2013; Hu et al. 2019). In order to validate the solutions for seismic case, the present solutions are compared with the results provided by Jiang et al. (2016) based on LEM. Table 4.10 shows the comparisons of F_s values for the slopes (of β=30°) having different rock properties (*GSI*, m_i and strength ratio) and subjected to different amount of horizontal seismic forces (i.e. k_h = 0.1, 0.2 and 0.3). This entire comparative study reveals a very interesting fact that irrespective of the rock slope properties, the estimated F_s values from the variational method are always smaller than the solutions obtained from the conventional LEM approach where the shape of the slip surface was required to pre-assume beforehand. For an example, slip surface was assumed to be circular by Shen et al. (2013), Lin et al. (2014), Huang et al. (2015), and Jiang et al. (2016).

Table 4.6 A comparison of F_s from the present analysis with the (i) limit equilibrium solutions of Carranza-Torres (2004), and Shen et al. (2013) and (ii) limit analysis solutions of Li et al. (2011) with k_h=0

Input Parameters	Example1	Example2	Example3	Example4	Example6	Example7
σ_{ci} (MPa)	0.75	10	13.5	5.4	0.625	46
GSI	100	30	30	20	80	50
m_i	10	8	5	20	15	35
D_f	0	1	0.7	0.7	0.3	1
γ (kPa)	25	23	27	27	25	23
h (m)	27	50	50	25	25	250
β (deg.)	45	60	45	45	75	60
Factor of safety						
Present Study	2.20(2.26)*	0.40(0.44)	0.72(0.73)	0.83(0.85)	0.91(1.17)	1.11(1.38)
Carraza-Torres (2004)	3.14	0.44	1.0	1.20	–	–
Li et al. (2011)	13.89	0.17	1.0	1.33	–	–
Shen et al. (2013)	–	–	–	–	1.058 [1.045]**	1.402 [1.391]

Note:* The values within and outside the parenthesis are obtained by using the equivalent cohesion and friction angle as prescribed by Hoek et al. (2002) and Li et al. (2008), respectively.
** The values within the brackets are computed by Shen et al. (2013) using SLIDE 6.0.

Table 4.7 A comparison of F_s from the present analysis with the (i) limit analysis solutions of Li et al. (2008) and (ii) limit equilibrium solutions of Dong-Ping et al. (2017) with k_h=0

β (deg.)	m_i	$(\sigma_{ci}/(\gamma h))_{cr}$	Present study	Li et al. (2008)	Dong-Ping et al. (2017)
30	5	0.070	0.684 (0.694)	1.0	0.992
	15	0.026	0.706 (0.718)	1.0	1.003
	25	0.016	0.707 (0.725)	1.0	1.010
	35	0.011	0.689 (0.714)	1.0	0.994
45	5	0.135	0.725 (0.721)	1.0	0.989
	15	0.058	0.771 (0.745)	1.0	0.990
	25	0.036	0.794 (0.751)	1.0	0.990
	35	0.026	0.800 (0.753)	1.0	0.991
60	5	0.232	0.756 (0.793)	1.0	1.006
	15	0.130	0.770 (0.861)	1.0	0.995
	25	0.088	0.782 (0.878)	1.0	0.991
	35	0.066	0.787 (0.886)	1.0	0.990

Note: The values within and outside the parenthesis are obtained by using the equivalent cohesion and friction angle as prescribed by Hoek et al. (2002) and Li et al. (2008), respectively.

In the present analysis, there was no such prior requirement. The present computed slip surfaces, which appear to be quadratic in all the regions, are further compared with the available (a) circular and arbitrary slip surfaces provided by Dong-Ping et al. (2017) through the application of the limit equilibrium method (LEM) and (b) plastic zones presented by Li et al. (2008), considering the finite element limit analysis (FELA) approach and are depicted in Fig. 4.9. Therefore, the shape of the slip surface obtained from the present study diverges significantly from those presented by Li et al. (2008) and Dong-ping et al. (2017). The present computed slip surfaces seem to encompass larger mass of soil; this eventually indicates larger driving force and, hence, lowers estimation of F_s through variational method.

Table 4.8 A comparison of F_s from the present analysis with the limit equilibrium solutions of Lin et al. (2014) and Huang et al. (2015) with k_h=0 for different *GSI* and m_i

		Constant m_i varying *GSI*					Constant *GSI* varying m_i				
h (m)	β (deg.)	m_i	*GSI*	Present study	Lin et al. (2014)	Huang et al. (2015)	*GSI*	m_i	Present study	Lin et al. (2014)	Huang et al. (2015)
20	63	17	10	1.07 (1.47)	0.36	--	50	5	5.89 (5.98)	7.48	--
			30	2.29 (3.08)	1.33	--		10	5.19 (5.56)	6.93	--
			50	4.87 (5.56)	4.94	--		20	4.80 (5.61)	7.07	--
			70	13.88 (14.12)	18.34	--		25	4.74 (5.71)	7.20	--
			100	108.68 (108.56)	--	--		30	4.70 (5.83)	7.33	--
40	45	10	10	0.90 (0.93)	--	1.16	30	5	1.16 (1.21)	--	1.24
			30	1.43 (1.53)	--	1.43		10	1.43 (1.53)	--	1.72
			50	1.94 (2.11)	--	2.13		20	1.75 (1.92)	--	2.34
			70	2.89 (3.05)	--	2.95		25	1.87 (2.06)	--	2.62
			100	8.76 (8.71)	--	9.09		30	1.96 (2.18)	--	2.82

Note: The values within and outside the parenthesis are obtained by using the equivalent cohesion and friction angle as prescribed by Hoek et al. (2002) and Li et al. (2008), respectively.

Table 4.9 A comparison of F_s from the present analysis with the solutions of Chen and Lin (2019) obtained by using gravity increase method for k_h=0

Varying σ_{ci} / *GSI* / m_i		10	14	18	22	26	30
Changing σ_{ci} (for *GSI*=20, m_i =15,D_f =0.7)	Present Study	0.72(0.86)* 0.58(0.68)	0.79(0.96) 0.64(0.76)	0.85(1.05) 0.69(0.83)	0.90(1.12) 0.74(0.89)	0.94(1.18) 0.77(0.94)	0.98(1.24) 0.81(0.99)
	Chen and Lin [30]	1.21 0.75	1.48 0.93	1.71 1.08	2.01 1.24	2.24 1.38	2.45 1.51
Changing *GSI* (for σ_{ci}=20MPa, m_i =15,D_f =0.7)	Present Study	0.57(0.68) 0.47(0.54)	0.69(0.84) 0.57(0.67)	0.81(1.01) 0.67(0.80)	0.93(1.17) 0.76(0.92)	1.05(1.33) 0.86(1.05)	1.17(1.49) 0.95(1.18)
	Chen and Lin [30]	0.81 0.50	1.18 0.73	1.6 1.01	2.16 1.34	2.84 1.71	3.59 2.18
Changing m_i (for σ_{ci}=20MPa, *GSI*=20,D_f =0.7)	Present Study	0.77(0.93) 0.62(0.73)	0.86(1.06) 0.70(0.84)	0.93(1.16) 0.76(0.92)	0.98(1.25) 0.81(1.00)	1.04(1.33) 0.86(1.06)	1.08(1.39) 0.90(1.12)
	Chen and Lin [30]	1.40 0.87	1.76 1.10	2.16 1.34	2.51 1.55	2.85 1.75	3.20 1.96

Note: (a)* The values within and outside the parenthesis are obtained by using the equivalent cohesion and friction angle as prescribed by Hoek et al. (2002) and Li et al. (2008), respectively.

(b) The values of F_s on the numerator and the denominator are reported for h=20m and h=40m, respectively.

Table 4.10 A comparison of F_s from the present analysis with the limit equilibrium solutions of Jiang et al. (2016) for 30° slope with different k_h

			k_h=0		k_h=0.1		k_h=0.2		k_h=0.3	
$\sigma_{ci}/(\gamma h)$	*GSI*	m_i	Present study	Jiang et al. (2016)	Present study	Jiang et al. (2016)	Present study	Jiang et al. (2016)	Present study	Jiang et al. (2016)
1	20	5	0.57 (0.60)	0.80	0.46 (0.50)	0.62	0.38 (0.40)	0.58	0.32 (0.33)	0.42
		20	1.03 (1.03)	1.40	0.84 (0.84)	1.20	0.70 (0.70)	1.00	0.59 (0.60)	0.82
		35	1.28 (1.28)	1.79	1.04 (1.04)	1.42	0.87 (0.87)	1.20	0.73 (0.73)	1.00
20	60	5	3.85 (3.80)	5.80	3.13 (3.10)	4.90	2.61 (2.56)	4.00	2.21 (2.16)	3.30
		20	4.64 (4.75)	6.40	3.77 (3.90)	5.20	3.14 (3.22)	4.40	2.64 (2.72)	3.60
		35	5.19 (5.39)	7.10	4.22 (4.40)	6.00	3.50 (3.70)	5.00	2.95 (3.10)	4.20
40	100	5	40.50 (40.29)	62.00	31.41 (31.24)	46.00	24.71 (24.58)	35.00	19.62 (19.50)	29.00
		20	25.51 (25.35)	40.00	20.17 (20.01)	30.00	16.27 (16.11)	24.00	13.34 (13.18)	18.00
		35	22.00 (21.88)	36.00	17.57 (17.42)	28.00	14.34 (14.17)	21.00	11.92 (11.73)	21.00

Note: The values within and outside the parenthesis are obtained by using the equivalent cohesion and friction angle as prescribed by Hoek et al. (2002) and Li et al. (2008), respectively.

(a)

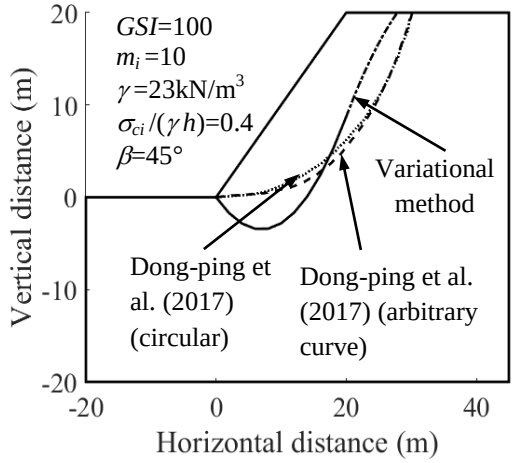

(b)

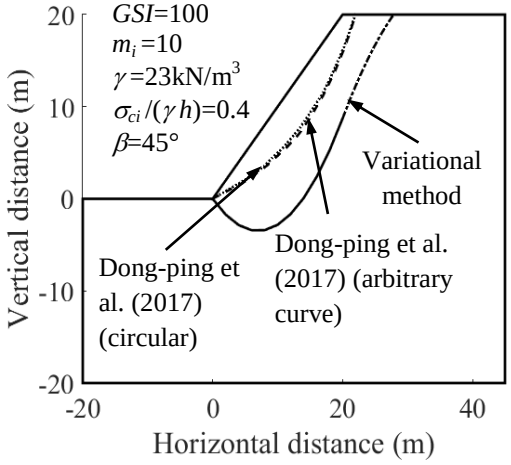

(c)

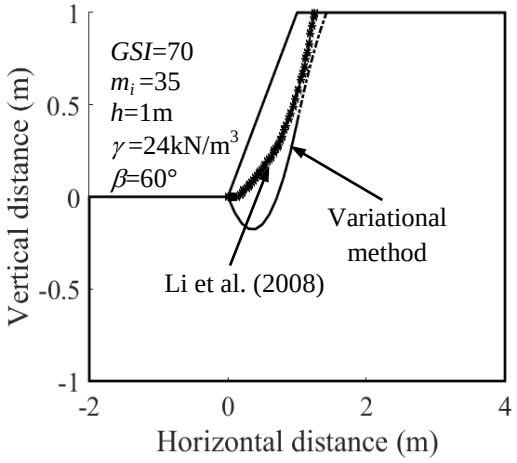

Fig. 4.9 Comparison of the obtained critical slip surfaces with the prescribed slip surface provided by (a) Dong-ping et al. (2017) considering deep slip surface, (b) Dong-ping et al. (2017) considering shallow slip surface, and, (c) Li et al. (2008).

4.7 SUMMARY

In the present chapter, formulations based on the variational method are presented for calculating the factor of safety of rock slopes subjected to seismic accelerations. The pseudostatic method is adopted and the stability charts in terms of factor of safety are provided for the following six parameters (i) slope geometry (β, h), (ii) material properties of the rock mass (GSI, σ_{ci} and m_i) and (iii) seismic acceleration coefficient (k_h). The influences of each of the parameters are studied thoroughly. The critical failure surfaces are plotted for several different cases. The obtained present solutions are compared with the available solutions in the literature. The design charts provided in this chapter will be useful to the practicing engineers for assessing the stability of the rock slopes.

4.8 LIMITATIONS

The variational method, based on the principles of the Limit Equilibrium Method (LEM), inherits certain drawbacks from LEM. These include the neglect of stress-strain and strain-displacement relationships, the inability to handle complex geometries, arbitrary boundary conditions, intricate loading conditions, and variations in soil properties. As a result, the present solutions lack precision and cannot be definitively regarded as either upper or lower bounds on the true collapse load. The proposed formulations exclusively rely on strength parameters, making the computed F_s values insensitive to stiffness parameters. Moreover, the slope is considered to be homogenous, single stage and having a constant factor of safety along the entire slip surface. For high slopes, consideration of multiple stages would provide the stability values for more realistic scenarios. Furthermore, the presented stability charts are applicable only within specified parameter ranges.